Supporting Information

Surface Enrichment in Equimolar Mixtures of Non-Functionalized and Functionalized Imidazolium-Based Ionic Liquids

Bettina S. J. Heller, Claudia Kolbeck, Inga Niedermaier, Sabine Dommer, Jürgen Schatz, Patricia Hunt, Florian Maier, and Hans-Peter Steinrück

SUPPORTING INFORMATION

IL1: 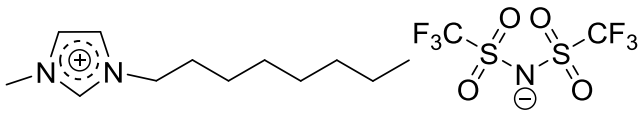

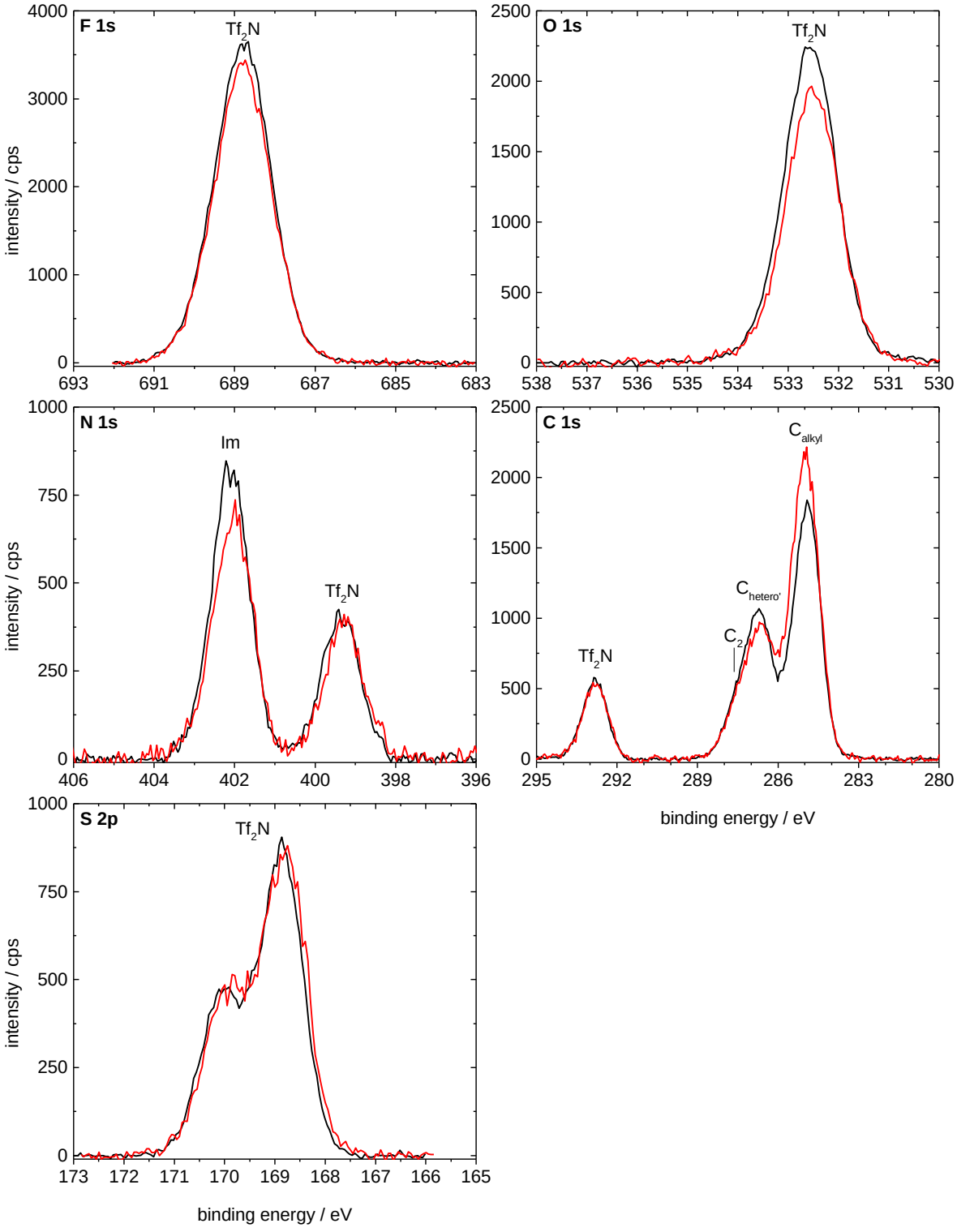

Figure S1: F 1s, O 1s, N 1s, C 1s, and S 2p spectra of IL1, $[C_8C_1Im][Tf_2N]$, in 0° (black) and 80° (red) emission, measured with Al K_α radiation.

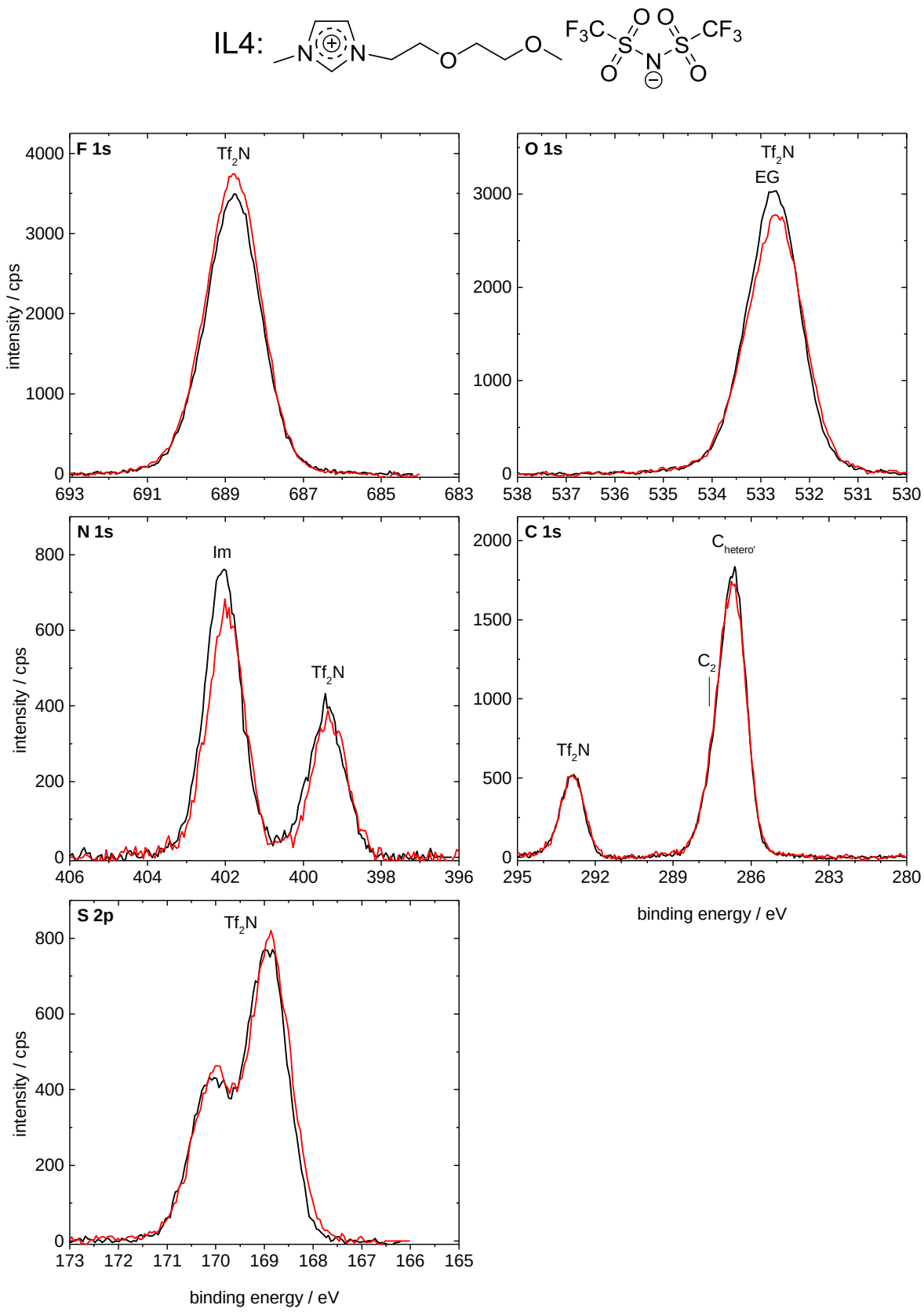

Figure S2: F 1s, O 1s, N 1s, C 1s, and S 2p spectra of IL4, $[Me(EG)_2C_1Im][Tf_2N]$, in 0° (black) and 80° (red) emission, measured with Al K_α radiation.

Table S1: Quantitative analysis of the 0° and 80° emission XP spectra of IL1, $[C_8C_1Im][Tf_2N]$. The nominal and experimentally determined composition is given for all elements contained in the IL. The ASFs are taken from ref [44].

	F 1s F_{Tf2N}	**O 1s** O_{Tf2N}	**N 1s** N_{Im}	**N 1s** N_{Tf2N}	**C 1s** C_{Tf2N}	**C 1s** C_2	**C 1s** $C_{hetero'}$	**C 1s** C_{alkyl}	**S 2p** S_{Tf2N}
ASF	1.00	0.67	0.46	0.46	0.30	0.30	0.30	0.30	0.64
nominal	6	4	2	1	2	1	4	7	2
binding energy / eV	688.8	532.6	402.1	399.4	292.8	287.6	286.7	284.9	169.5
corrected intensity 0°	6468	4462	2146	1077	2158	1113	4452	7483	2196
atom ratio 0°	5.9	4.1	2.0	1.0	2.0	1.0	4.1	6.9	2.0
corrected intensity 80°	6067	3902	1892	1036	2122	1030	4120	9150	2254
atom ratio 80°	5.6	3.6	1.8	1.0	2.0	1.0	3.8	8.4	2.1

Table S2: Quantitative analysis of the 0° and 80° emission XP spectra of IL2, $[C_8C_1Im][PF_6]$. The nominal and experimentally determined composition is given for all elements contained in the IL. The ASFs are taken from ref [44].

	F 1s F_{PF6}	**N 1s** N_{Im}	**C 1s** C_2	**C 1s** $C_{hetero'}$	**C 1s** C_{alkyl}	**P 2p** P_{PF6}
ASF	1.00	0.46	0.30	0.30	0.30	0.46
nominal	6	2	1	4	7	1
binding energy / eV	686.8	402.2	287.7	286.8	285.1	137.1
corrected intensity 0°	18773	5890	3023	12092	20328	3329
atom ratio 0°	6.2	2.0	1.0	4.0	6.7	1.1
corrected intensity 80°	15245	4980	2683	10732	26599	3041
atom ratio 80°	5.0	1.7	0.9	3.6	8.8	1.0

Table S3: Quantitative analysis of the 0° and 80° emission XP spectra of IL3, $[(MeO)_2Im][PF_6]$. The nominal and experimentally determined composition is given for all elements contained in the IL. The ASFs are taken from ref [44].

	F 1s F_{PF6}	**O 1s O_{MeO}**	**N 1s N_{MeO}**	**C 1s C_2**	**C 1s $C_{hetero'}$**	**P 2p P_{PF6}**
ASF	1.00	0.67	0.46	0.30	0.30	0.46
nominal	6	2	2	1	4	1
binding energy / eV	686.8	535.3	403.6	288.1	287.0	137.0
corrected intensity 0°	29478	9241	8535	4429	17715	5236
atom ratio 0°	6.3	2.0	1.8	1.0	3.8	1.1
corrected intensity 80°	28912	9290	8563	4519	18077	5265
atom ratio 80°	6.2	2.0	1.8	1.0	3.9	1.1

Table S4: Quantitative analysis of the 0° and 80° emission spectra of IL4, $[Me(EG)_2C_1Im][Tf_2N]$. The nominal and experimentally determined composition is given for all elements contained in the IL. The ASFs are taken from ref [44].

	F 1s F_{Tf2N}	**O 1s O_{EG}**	**N 1s N_{Im}**	**N 1s N_{Tf2N}**	**C 1s C_{Tf2N}**	**C 1s C_2**	**C 1s $C_{hetero'}$**	**S 2p S_{Tf2N}**
ASF	1.00	0.67	0.46	0.46	0.30	0.30	0.30	0.64
nominal	6	6	2	1	2	1	8	2
binding energy / eV	688.8	532.7	402.1	399.4	292.9	287.7	286.7	169.6
corrected intensity	6160	6216	1950	1007	1985	941	7527	1948
atom ratio 0°	6.2	6.3	2.0	1.0	2.0	1.0	7.6	2.0
corrected intensity 80°	6660	6047	1722	926	2026	1030	7382	2005
atom ratio 80°	6.7	6.1	1.7	0.9	2.0	1.0	7.5	2.0

Table S5: Quantitative analysis of the 0° and 80° emission XP spectra of the equimolar IL1+IL3 mixture, $[C_8C_1Im][Tf_2N]$+ $[(MeO)_2Im][PF_6]$, mixture. The nominal and experimentally determined composition is given for all elements contained in the IL mixture. The ASFs are taken from ref [44].

	F 1s F_{Tf2N}	**F 1s F_{PF6}**	**O 1s O_{MeO}**	**O 1s O_{Tf2N}**	**N 1s N_{MeO}**	**N 1s N_{Im}**	**N 1s N_{Tf2N}**	**C 1s C_{Tf2N}**	**C 1s $C_{2,Im}$**	**C 1s $C_{hetero',Im}$**	**C 1s C_{alkyl}**	**C 1s $C_{2,MeO}$**	**C 1s $C_{hetero',MeO}$**	**S 2p S_{Tf2N}**	**P 2p P_{PF6}**
ASF	1.00	1.00	0.67	0.67	0.46	0.46	0.46	0.30	0.30	0.30	0.30	0.30	0.30	0.64	0.46
nominal	6	6	2	4	2	2	1	2	1	4	7	1	4	2	1
binding energy / eV	688.8	686.7	535.3	532.6	403.6	402.0	399.4	292.8	287.5	286.6	284.9	288.1	287.0	169.4	137.0
corrected intensity 0°	3696	3254	987	2343	960	1271	599	1229	628	2513	4398	486	1945	1184	621
atom ratio 0°	6.4	5.6	1.7	4.0	1.7	2.2	1.0	2.1	1.1	4.3	7.6	0.8	3.4	2.1	1.1
corrected intensity 80°	4201	1969	645	2432	568	1252	632	1352	778	3113	6458	198	791	1313	453
atom ratio 80°	7.2	3.4	1.1	4.2	1.0	2.2	1.1	2.3	1.3	5.4	11.1	0.3	1.4	2.3	0.8

Table S6: Quantitative analysis of the 0° and 80° emission spectra of the equimolar IL2+IL3 mixture, $[C_8C_1Im][PF_6]$+$[(MeO)_2Im][PF_6]$ mixture. The nominal and experimentally determined composition is given for all elements contained in the IL mixture. The ASFs are taken from ref [44].

	F 1s F_{PF6}	**O 1s** O_{MeO}	**N 1s** N_{MeO}	**N 1s** N_{Im}	**C 1s** $C_{2,Im}$	**C 1s** $C_{hetero',Im}$	**C 1s** C_{alkyl}	**C 1s** $C_{2,MeO}$	**C 1s** $C_{hetero',MeO}$	**P 2p** P_{PF6}
ASF	1.00	0.67	0.46	0.46	0.30	0.30	0.30	0.30	0.30	0.46
nominal	12	2	2	2	1	4	7	1	4	2
binding energy / eV	686.8	535.4	403.6	402.1	287.6	286.7	285.0	288.2	287.1	137.0
corrected intensity 0°	19837	2742	2843	3364	1706	6824	11943	1469	5875	3514
atom ratio 0°	12.2	1.7	1.8	2.1	1.1	4.2	7.4	0.9	3.6	2.2
corrected intensity 80°	15674	1447	1596	3631	1660	6640	20230	1151	4602	3319
atom ratio 80°	9.6	0.9	1.0	2.2	1.0	4.1	12.5	0.7	2.8	2.1

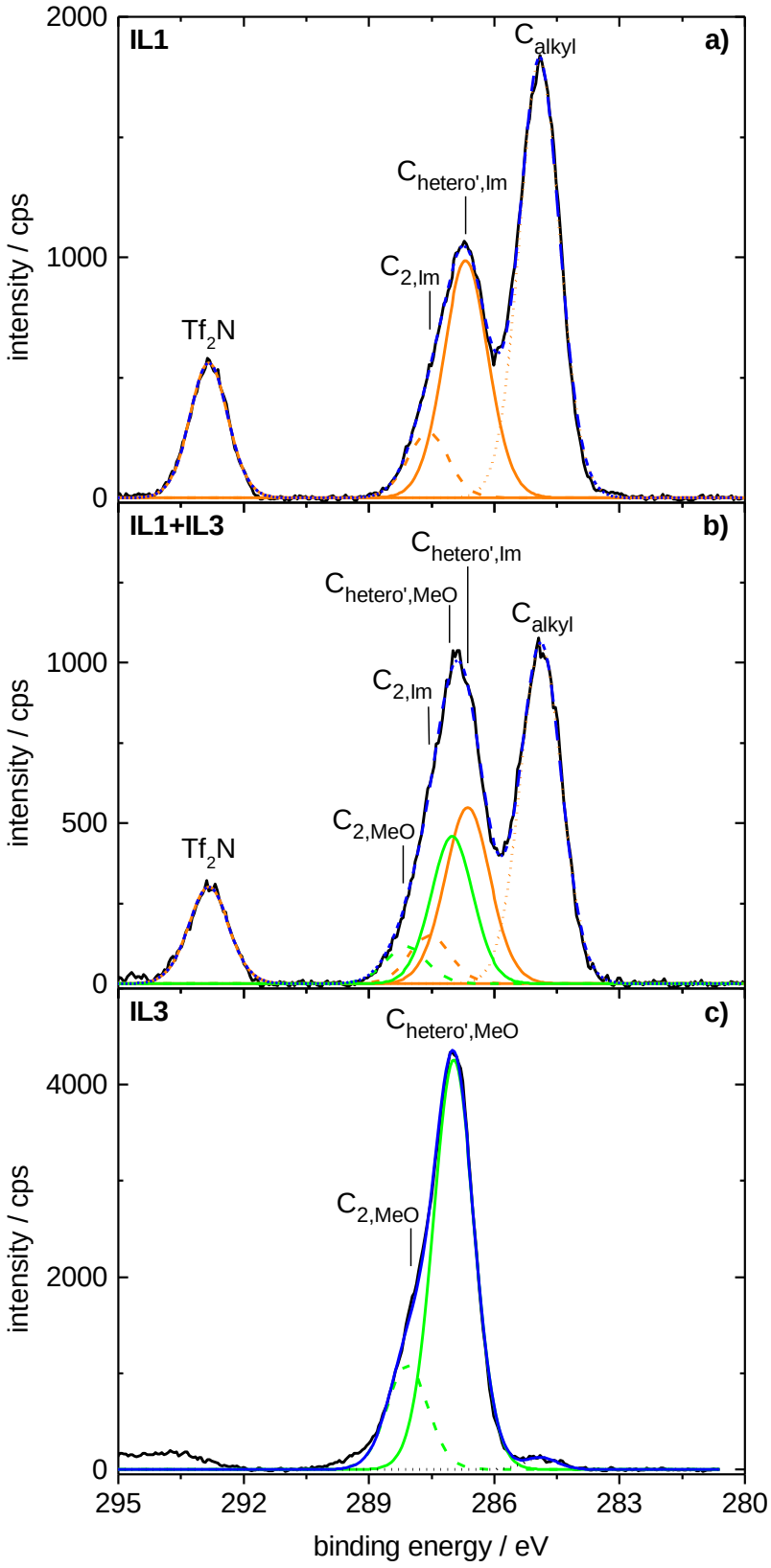

Figure S3: Fits of the C 1s spectra of a) IL1, b) equimolar IL1+IL3 mixture, and c) IL3 indicating all peaks fitted with the constraints mentioned in the Experimental Section.

DFT calculations and charge analysis:

$[(MeO)_2Im]^+$, $[C_2C_2Im]^+$, and $[Me(EG)_1C_1Im]^+$ can take on a range of structural conformers (see Figure S4). In $[(MeO)_2Im]^+$ and $[C_2C_2Im]^+$, the alkyl and methoxy arms can be positioned forward, backward, or perpendicular to the imidazolium ring. In $[Me(EG)_1C_1Im]^+$ the ether chain can be orientated all trans or it can wrap around such that the O_{EG} atom interacts with the H atoms of the imidazolium ring.

To ensure that all relevant conformers of $[C_2C_2Im]^+$ and $[(MeO)_2Im]^+$ have been located, a relaxed potential energy surface (PES) has been generated by systematically varying the torsion angles τ of the arms $\tau(C_2\text{-N-C-C})$ in $[C_2C_2Im]^+$ or $\tau(C_2\text{-N-O-C})$ in $[(MeO)_2Im]^+$ allowing for the relaxation of all other internal coordinates (see Figure S5). The angles τ have been rotated, in steps of 10º, through 360º. $[C_2C_2Im]^+$ exhibits four minima, $[(MeO)_2Im]^+$ exhibits only two minima due to instability of the in-plane orientations of the methoxy groups. For both cations, the “up-down” conformer has the lowest energy (ground state). For $[C_2C_2Im]^+$, the barrier for interconversion between the minima is very low and the alkyl arms will rotate freely in solution at room temperature. For $[(MeO)_2Im]^+$, the barriers for rotation are higher and more limited rotation is expected.

For the charge analysis we have selected the “up-down” (ground state) for both $[C_2C_2Im]^+$ and $[(MeO)_2Im]^+$. As the rotational profile for $[C_2C_2Im]^+$ is shallow, we have selected the transition state “front-back (TS)” as the second conformer for charge analysis. The minimum “up-front” (+1.2 kJ/mol) has been selected as the second conformer for analysis of $[(MeO)_2Im]^+$. Key conformer energies are reported in Table S7.

$[Me(EG)_1C_1Im]^+$ with its shorter side chain is used as model for the cation of $[Me(EG)_2C_1Im][Tf_2N]$ (IL4). The ether chain of $[Me(EG)_1C_1Im]^+$ can take a range of orientations, the two key torsion angles are $\tau_1=\tau(C_2\text{-N-C-C})$ and $\tau_2=\tau(\text{N-C-C-O})$; relaxed PESs for these angles are shown in Figure S6. Note the significantly different vertical energy scales between the PESs of Figure S5 and S6. The gauche geometries, with the ether chain rotated to interact with the imidazolium ring, are substantially more stable than the planar linear trans conformers. However, in solution it is anticipated that the ether chains can associate with adjacent cation molecules, and thus, planar linear conformations will be stabilized. Hence, both the gauche “folded” and trans “linear” conformers have been selected for charge analysis. Key conformer energies are reported in Table S8.

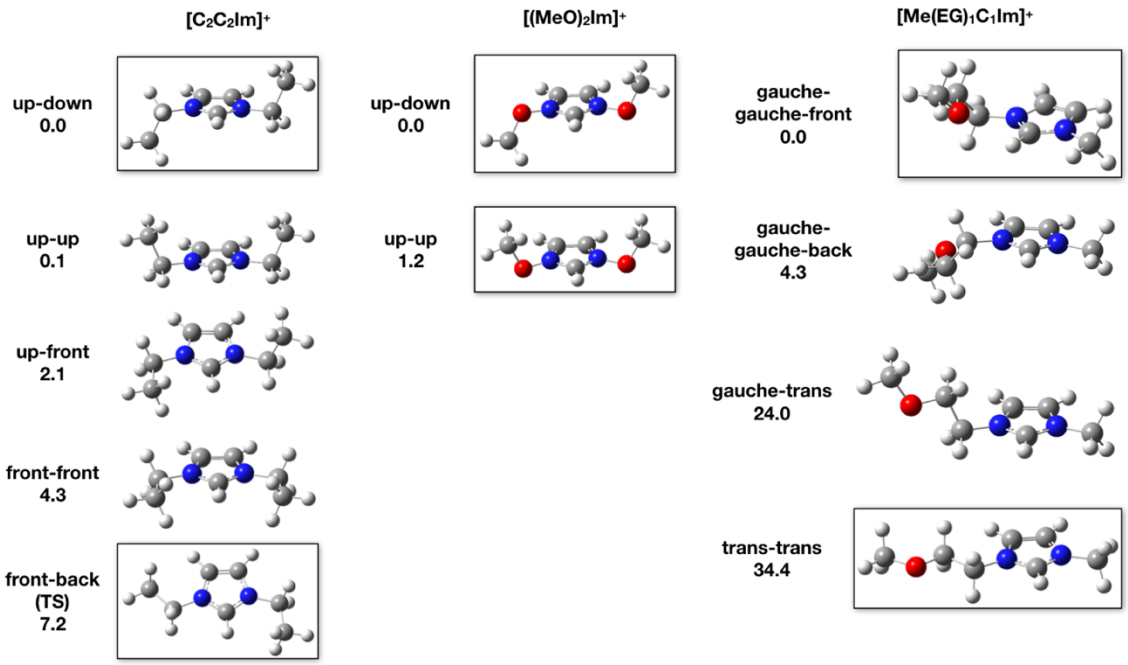

Figure S4: Optimized conformers of $[C_2C_2Im]^+$, $[(MeO)_2Im]^+$, and $[Me(EG)_1C_1Im]^+$ (energies in kJ/mol relative to the lowest-energy ground state); "boxed" conformers are those selected for charge analysis.

Table S7: Critical point energies in kJ/mol for $[(MeO)_2Im]^+$ and $[C_2C_2Im]^+$, * indicates a transition state structure, - indicates no critical point was located. Bold values indicate states of the discussed NBO and ChelpG analysis.

	$[(MeO)_2Im]^+$	$[C_2C_2Im]^+$
up-down	**0.0**	**0.0**
up-front	10.2*	2.1
up-up	**1.2**	0.1
front-front	-	4.3
up-back	9.2*	5.0*
front-back	-	**7.1***

Table S8: Critical point energies in kJ/mol for $[Me(EG)_1C_1Im]^+$ for the different conformers analyzed (torsion angles are also shown). Bold values indicate states of the discussed NBO and ChelpG analysis.

	τ_1, τ_2 (º)	$[Me(EG)_1C_1Im]^+$
gauche-gauche-front	61, -66	**0.0**
gauche-gauche-back	-117, -64	4.3
gauche-trans	99, 180	24.0
trans-trans	180, 180	**34.4**

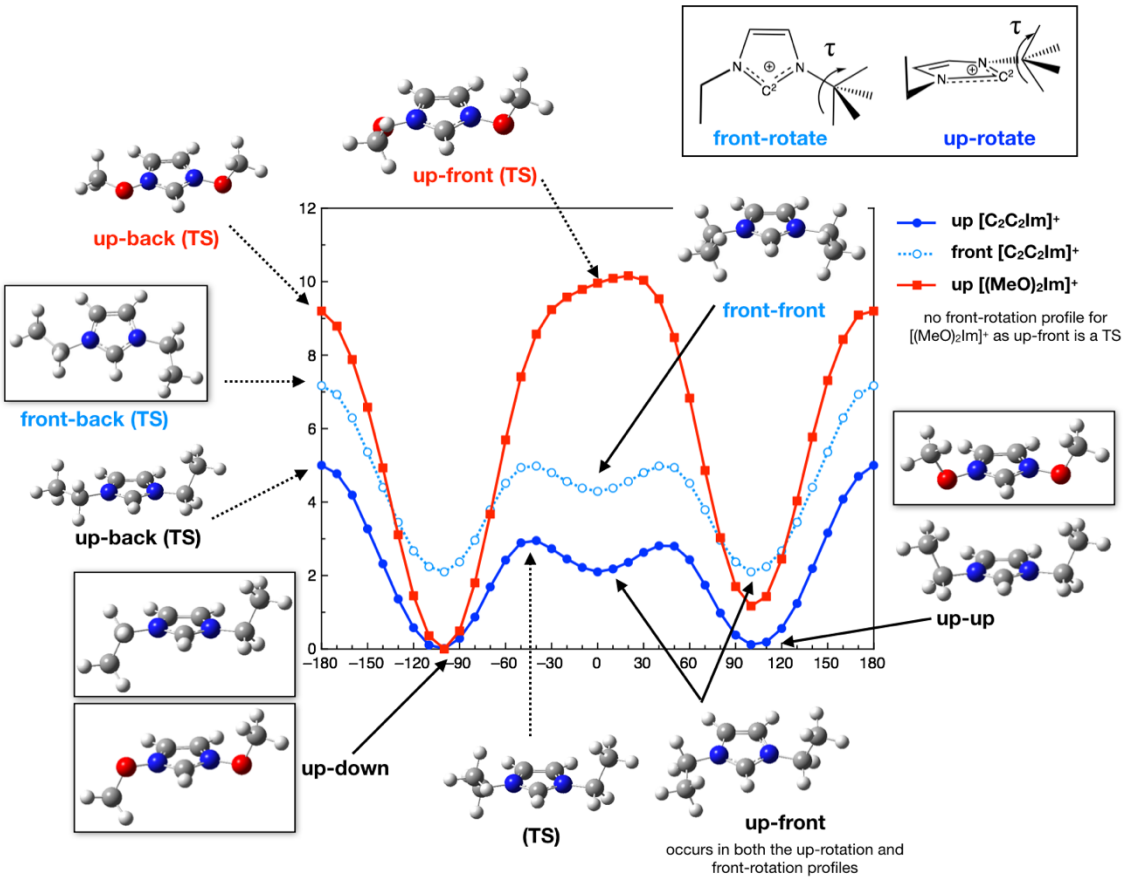

Figure S5: Relaxed scan of the alkyl/methoxy chain rotational potential energy surfaces, energy in kJ/mol.

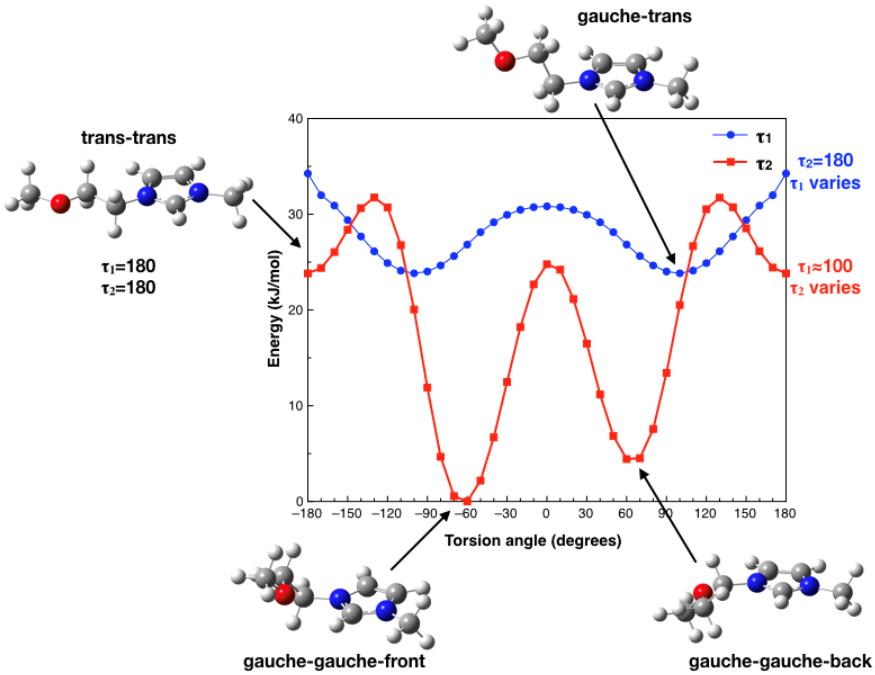

Figure S6: Relaxed scan for $[Me(EG)_1C_1Im]^+$ $\tau_1=\tau(C_2\text{-}N\text{-}C\text{-}C)$ and $\tau_2=\tau(N\text{-}C\text{-}C\text{-}O)$ angles, energy in kJ/mol.

Initial results from the NBO and ChelpG charge analysis are summarized in Table S9. The significantly different structures yield qualitatively similar results. Note that the maximum difference in the oxygen atom charges from $[(MeO)_2Im]^+$ to $[Me(EG)_1C_1Im]^+$ is more pronounced in the NBO analysis compared to the ChelpG analysis (NBO: +0.25 e vs. ChelpG: +0.13 e). NBO is known to produce larger charge polarization than ChelpG. The ChelpG charges are based on the external potential while the NBO charges are based on the electron density close to the atomic center. Thus, conceptually, the NBO method represents changes close to the nucleus, and thus, is expected to better reflect the core level orbitals probed by XPS. Nevertheless, charge analysis models should be considered as qualitative rather than quantitative; notably, in our analysis here, the two methods are qualitatively consistent. A visual representation NBO charges are depicted in Figure S7, where atoms are color coded on a scale from bright blue for negative through white (for neutral) to bright red for positive charge.

Table S9: NBO and ChelpG (in brackets) partial charge values in units of the elementary charge e for key atoms and groups, carried out for the conformers marked in Figure S4.

	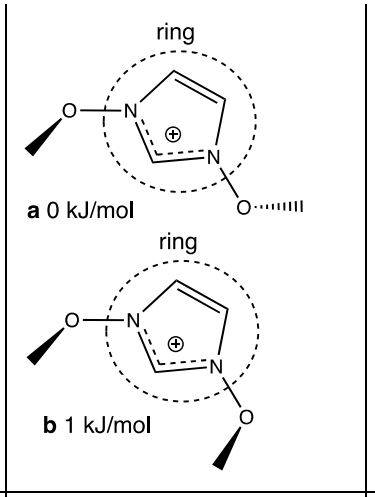		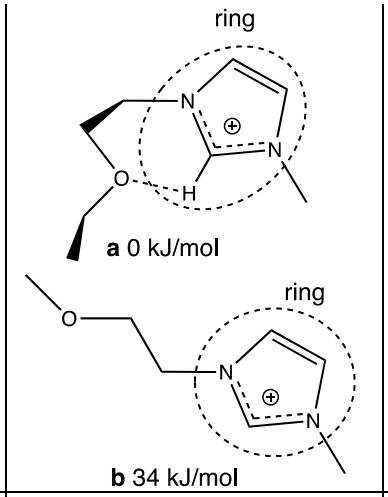		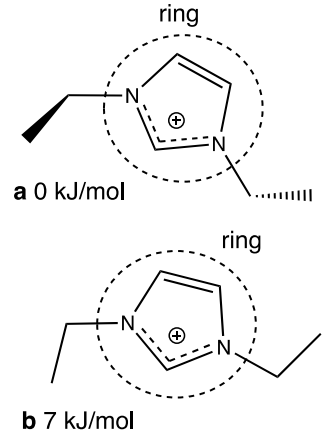	
	$[(MeO)_2Im]^+$		**$[Me(EG)_1C_1Im]^+$**		**$[C_2C_2Im]^+$**	
	a **up-down**	**b** **up-up**	**a**	**b**	**a** **up-down**	**b** **front-back (TS)**
N	-0.02 (+0.29)	-0.02 (+0.28)	-0.34 (+0.15)	-0.33 (+0.14)	-0.35 (+0.06)	-0.34 (+0.06)
O	-0.35 (-0.28)	-0.35 (-0.25)	-0.60 (-0.32)	-0.57 (-0.38)	-	-
ring	+0.93 (+0.92)	+0.93 (+0.92)	+0.34 (+0.57)	+0.34 (+0.56)	+0.31 (+0.46)	+0.32 (+0.43)

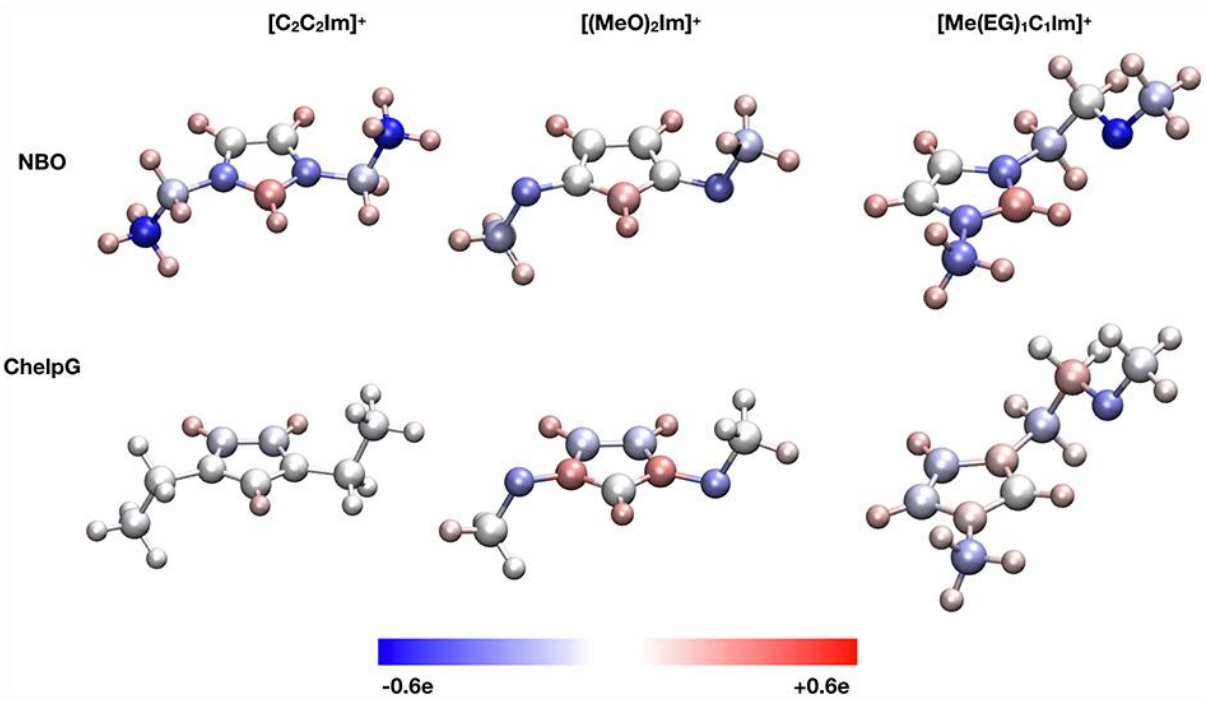

Figure S7: Pictorial representation of charge distribution in the lowest energy conformers of $[C_2C_2Im]^+$, $[(MeO)_2Im]^+$, and $[Me(EG)_1C_1Im]^+$ with color ranging from bright blue (-0.6 e) through white (neutral) to bright red (+0.6 e).

Discussion of the NBO vs. the ChelpG charge analysis methods.

While the results of the NBO and ChelpG analysis are both termed "charges" they report on different aspects of the electronic structure. The NBO method identifies the localized electron density at atomic sites. The ChelpG method, in contrast, is based on the electrostatic potential (ESP) far from the atoms (evaluated beyond the van der Waals radius). While fitted trends may show a good correlation with both NBO and ChelpG there are concerns with the ChelpG charges which lead us to focus primarily on the NBO charges. There are three reasons why the ChelpG charges have not been the focus of attention: concerns with the physical underpinning of the ChelpG analysis, concerns that charges are unreliable for buried atoms using the ChelpG analysis and concerns regarding the conformer dependence of ChelpG charges. Each of these is discussed further below.

Concerns with the physical underpinning of the ChelpG analysis

The charge obtained from fitting an ESP close to atomic centers is unreliable, this is why the ESP data points are taken from beyond the van der Waals radii of the atoms. However, the XPS technique employed here is probing the core orbitals of an atom. Thus, the influence of these states on the ESP is strongly shielded. The NBO method is a localized method, which explicitly includes core electron density. Thus, while fitted trends may show a good

correlation with both NBO and ChelpG there is a more robust physical basis for the correlation of the NBO charges with the experimental data.

Concerns with the "buried atom" conformation of the ChelpG analysis

Based on previous studies comparing XPS spectra to ChelpG charges, significant conformer dependence was determined for conformers with the charge-bearing atom buried or exposed within an IL ion-pair. In the documented case, a S atom showed a conformer-based charge variation of 0.5e.[1] The NBO charges were established as more reliable in this respect. Thus, while the ChelpG charges for the trans $[Me(EG)_1C_1Im]^+$ conformer can be considered reasonably reliable, those for the internal H-bonding gauche $[Me(EG)_1C_1Im]^+$ conformer (with the buried O atom) cannot be considered as reliable, weakening the possibility that the lower charge is physically reasonable.

A choice made on which conformers to focus upon in the analysis

The NBO and ChelpG charges for the lowest energy conformers of N-O-Me oxygen (-0.35 e, -0.28 e) vs. those for N-CH_2-CH_2-O-Me oxygen (-0.60 e, -0.32 e) exhibit a difference of (-0.25 e, -0.04 e). However, we do not believe this is the best comparison to make. Conformer **b** for $[(MeO)_2Im]^+$ is essentially iso-energetic with conformer **a** at the level of theory applied. Both conformers can expected to be present at the same concentration, thus, taking the average charge between these two conformers is reasonable. Thus, for N-O-Me, the average charges on oxygen in $[(MeO)_2Im]^+$ to be considered are -0.35 (NBO) and -0.27 e (ChelpG).

Internal H-bonding is expected to be maximized for the isolated $[Me(EG)_1C_1Im]^+$ cations, however, this is not expected in a liquid environment: The O atom can H-bond with other cations and the imidazoilium C_2-H can associate with the anion. Moreover, alkyl chain aggregation can be expected as nano-scale domains are well known to form in ILs; computed rotational profiles for the ethylene-glycol arm indicated movement was accessible at room temperature. Hence, we did not expect the internal H-bonding gauche $[Me(EG)_1C_1Im]^+$ cation to predominate in the IL, rather the trans-conformer **b** will be of increased importance. Thus, for $[Me(EG)_1C_1Im]^+$, the charges to be considered are -0.59 (NBO) and -0.35 e (ChelpG) where 0.35 e is the average of the gauche and trans conformer charges of -0.32 and -0.38 e, respectively.

Given the assumptions made above, the NBO and ChelpG average charges for N-O-Me oxygen (-0.35 e, -0.27 e) in $[(MeO)_2Im]^+$ vs. those for N-CH_2-CH_2-O-Me in $[Me(EG)_1C_1Im]^+$ (-0.57 e, -0.35 e) *exhibit a difference of -0.22* and -0.08 e. NBO charges are known to be more "polarized" than ChelpG charges which is reflected in the results obtained here. Nevertheless, the *qualitative trend* is that the charge on the oxygen atoms of $[(MeO)_2Im]^+$ is

less negative than for $[Me(EG)_1C_1Im]^+$. This qualitative interpretation is strengthened by the strong difference observed in XPS binding energies.

To further investigate environmental effects, "buried charge" and conformer dependence, additional supporting calculations have been carried out.

To extend the ion gas phase calculations, a continuum solvation model for ILs introduced by Bernales and co-workers, that is, the so-called “generic ionic liquid solvation model based on density” (GIL-SMD),[1] has been employed. Each of the gas-phase optimized cations discussed above has been placed into the continuum medium and evaluated. Where available, values specific to the $[PF_6]^-$ anion have been used (i.e. beta value, number of halogen atoms); the specific GIL-SMD parameters employed are: eps = 11.50, epsinf = 2.0449, SurfaceTensionAtInterface = 61.24, HBondAcidity = 0.229, HBondBasicity = 0.265, CarbonAromaticity = 0.188, ElectronegativeHalogenicity = 0.375. For details on the GIL-SMD, and parameter definitions see ref [1].

Moreover, gas-phase calculations were carried out on isolated cation-$[PF_6]^-$ ion pairs for all three imidazolium cations. The lowest energy cation conformers with $[PF_6]^-$ placed in the front and top positions (known lowest energy conformers for imidazolium based ILs) have been sampled. Typically, the larger and more diffuse the anion, the more pronounced the preference for the anion-pi "top" conformer over the H-bonding "front in-plane" interaction. For each cation investigated here, $[PF_6]^-$ was found to be unstable in the front position, and the ion-pair structures optimized to $[PF_6]^-$ in a top position. Final low-energy structures are depicted in Figure S8.

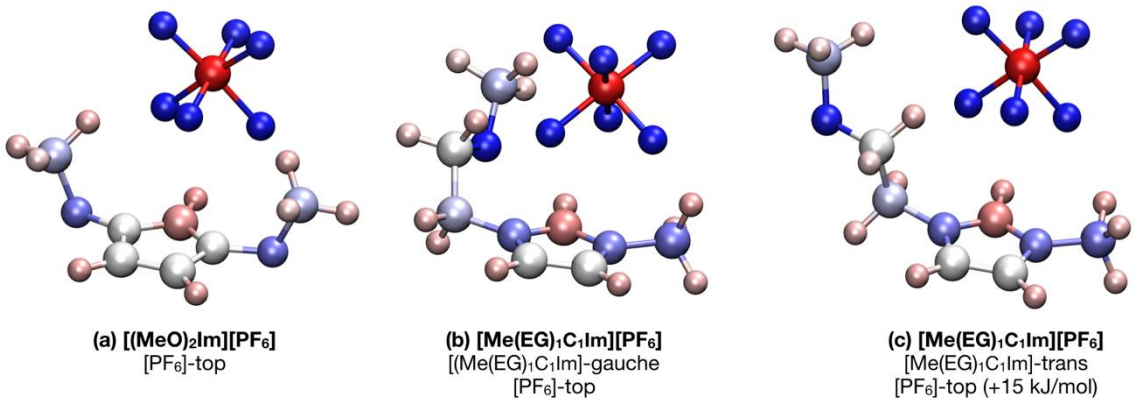

Figure S8: A color mapped representation of the NBO charges for (a) $[(MeO)_2Im][PF_6]$ (b) gauche-$[Me(EG)_1C_1Im][PF_6]$ and (c) trans-$[Me(EG)_1C_1Im][PF_6]$. Color scale is bright red (+0.6 e) through white to bright blue (-0.6 e).

The NBO (ChelpG) charges on the oxygen atoms for the gas-phase, GIL-SMD, and explicit ion-pair calculations are given in Table S10. The NBO charge varies very little between the different conformers, if a continuum solvation environment is included or not, or if explicit ion-pairs are considered or not. The ChelpG charges show a tendency to move towards more negative values on going from the gas phase, through continuum solvation, to explicit ion-pairing. Thus, the more sophisticated calculations (employing an SMD or ion-pair model) add additional support to the gas-phase based conclusion that the charge of the oxygen atoms is more negative in $[Me(EG)_1C_1Im]^+$ compared to $[(MeO)_2Im]^+$.

Table S10: Oxygen atom partial charges in units of e derived from NBO (in brackets: ChelpG charges) of the isolated cations in the gas-phase, of the cations in the continuum solvation environment (GIL-SMD), and of the ion pairs in the gas phase; values are given for the most-relevant configurations.

O charge NBO (ChelpG)	gas-phase	GIL-SMD	ion-pair $[PF_6]^-$
$[(MeO)_2Im]^+$	-0.35 (-0.28)	-0.37 (-0.32)	-0.36 (-0.32)
$[Me(EG)_1C_1Im]^+$ trans	-0.57 (-0.38)	-0.59 (-0.43)	-0.58 (-0.48)
$[Me(EG)_1C_1Im]^+$ gauche	-0.60 (-0.32)	-0.61 (-0.34)	-0.60 (-0.47)

[1] V. S. Bernales, A. V. Marenich, R. Contreras, C. J. Cramer and D. G. Truhlar, *J. Phys. Chem. B*, 2012, **116**, 9122–9129.